European Rotorcraft Forum

EFFECT OF AERODYNAMIC INTERFERENCE TO TAIL PROPELLER ON A COMPOUND HELICOPTER

Keita Kimura, kimura.keita@jaxa.jp, Japan Aerospace Exploration Agency (JAXA), (Japan)

Hideaki Sugawara, sugawara.hideaki@jaxa.jp, JAXA, (Japan)

Yasutada Tanabe, tanabe.yasutada@jaxa.jp, JAXA, (Japan)

Abstract

Computational Fluid Dynamics (CFD) simulations are conducted focusing on a tail propeller on a conceptual model of a high-speed compound helicopter proposed by JAXA. Since a number of components such as fixed wing and propellers are added to a conventional helicopter, it is important to understand the aerodynamic interactions between the components. In this paper, the influence of aerodynamic interactions on the performance of the tail propeller with the main rotor and fuselage, and the influence on the fuselage drag from the tail propeller, are investigated. The propeller performance tends to improve when subjected to the main rotor wake, however, the effect becomes trivial as the advance ratio increases. As for the interaction between the fuselage and the propeller, it is shown that the propeller performance placed in the shadow of a fuselage improves instead of increasing the drag of the fuselage due to the induced flow by the propeller. After considering these conflicting effects, it was found that although they cancel each other out in terms of thrust and drag, the propeller efficiency itself has a large possibility of decreasing during high-speed flight.

1. INTRODUCTION

To increase the cruising speed of helicopters and other VTOL aircraft, research and development of new rotorcraft configurations is being actively pursued worldwide. One of the most promising high-speed helicopter configurations is the compound helicopter, which is a conventional helicopter added with a fixed wing and propellers. Sikorsky is developing the Raider [1] and SB-1 Defiant [2] following the successful technology demonstration by the X2 [3], which are equipped with coaxial rotors and tail propellers. At the same time, Airbus Helicopters is developing the RACER, which is equipped with a box wing and propulsion propellers on the wing tips, following the speed-recording breaking demonstration of X3 [4]. JAXA has been researching a compound helicopter with a unique configuration, mainly targeting implementation as an emergency medical service (EMS) helicopter [5]. JAXA proposes a low-drag streamlined fuselage with a single main rotor, side propellers for anti-torque at both fixed wing tips, and a tail propeller for propulsion at the rear of the fuselage. As a performance target, it is aimed to maintain the weight of a conventional EMS helicopter (3000~4000 kg) and to approximately double the cruise speed to 500 km/hr.

To achieve the aforementioned compound helicopter, there are some technical issues to be solved. One of them is the problem of mutual interactions due to the addition of aerodynamic elements such as fixed wing and tail propeller. For example, it has been pointed out that the effect of the main rotor wake on each component varies greatly with flight speed. This is mainly due to the fact that the advection direction of the main rotor wake changes significantly with flight speed, and Stokkermans confirmed this on CFD [6]. Under hovering to low-speed flight conditions, the rotor wake directly interferes with the fixed wings and side propellers, and there is a concern about the effect on propeller performance even under cruise conditions. As for the aerodynamic interactions between the main rotor wake and the fixed wing, the generation of downloads to the fixed wing due to downwash has been discussed [7]. JAXA is also studying the design of an appropriate fixed wing installation in consideration of interference [8].

In this paper, aerodynamic interactions of a tail propeller with the main rotor and with the fuselage are investigated numerically. The changes in propeller thrust and efficiency at the assumed advance ratio are investigated, and the mechanism by which these changes occur between the components is discussed. This study would help to identify issues to be considered in the design of the tail propeller in consideration of the entire airframe system.

2. METHODOLOGIES

2.1. CFD solver

Simulations are performed using rFlow3D, a CFD solver for rotorcraft developed by JAXA. The calculation conditions used in this analysis are shown in Table 1. The moving overlapped grid method provides a direct representation of the rotor

Presented at 47th European Rotorcraft Forum, United Kingdom, 7-9th September, 2021

blade motion. FCMT [9], a spatial fourth-order accurate reconstruction method, and mSLAU [10] [11], an all-speed scheme, are used to achieve high order accuracy and low dissipation in a wide range of Mach numbers in structured grids. For the analysis of unstructured grids to reproduce complex shapes, FaSTAR [12] is used, where the spatial second-order MUSCL is used for higher accuracy, and the flux is evaluated by calculating the spatial gradient using the Green-Gauss method and stabilizing it using Hishida's method.

Since simulations are performed on a model scale at this time, and the Reynolds number is about one-order smaller than that of the full scale, a quasi-DNS (QDNS), which models turbulent viscosity with numerical viscosity introduced during discretization is used as a turbulence model to avoid excessive turbulent viscosity. In addition, a trim analysis function [13] is provided to control the forces and moments around the axes acting on each coordinate axis to match the target values, enabling accurate simulation of actual flight conditions.

Table 1 : Numerical methodologies in rFlow3D

Governing equations	Three-dimensional compressible Navier-Stokes equations
Spatial discretization	Finite volume method
Time integration	4 stages Runge-Kutta (Background) Dual-time stepping, LU-SGS (Blade, Fuselage)
Viscous terms	2nd order central difference method
Reconst-ruction	Structured grid : FCMT (Fourth-order compact MUSCL TVD)
	Unstructured grid : MUSCL+Green-Gauss with Hishida's limiter
Advection terms	mSLAU (modified SLAU)
Turbulence model	QDNS (quasi-DNS)

2.2. Simulation setup

Numerical simulations are conducted for HERACLES (Highly-efficient and rapid compound helicopter for experimental study), a downscaled model manufactured by JAXA for testing purposes. Table 2 shows the specifications of the components of HERACLES. To focus on the aerodynamic interactions of the tail propeller in this study, a simplified model was prepared as shown in Figure 1. To confirm the effects of the main rotor and fuselage, which have a large potential to affect the performance of the tail propeller, the results of these interference cases (TP/MR, TP/Fuse) are compared with those of the isolated tail propeller (TP_iso) and fuselage analyses (Fuse_iso). Although it has not yet been studied in this paper, it is planned to simulate the entire aircraft so that the main rotor and fuselage interfere with the tail propeller simultaneously.

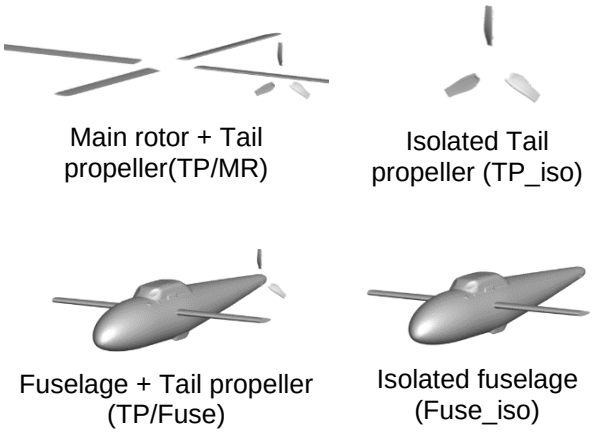

Figure 1 : configurations to investigating interactions between the tail propeller and other components (Main rotor, Fuselage)

Table 2 : Specifications of JAXA Model Helicopters (HERACLES)

Diameter of main roto D_{MR}	1.53 m
Diameter of tail propeller D_{TP}	0.25 m
Tail propeller center position (The center of the main rotor is used as the original point. Unit m)	(0.843, 0, -0.18)
Rotational speed (main rotor)	1250 rpm
Rotational speed (tail-propeller)	12000 rpm
span of fixed wing L	1.057 m
Gross weight	10.2 kg

The operating conditions used in the simulations are set based on HERACLES (Table 3). Inflow speed is set assuming that the advance ratio is about the same as that of conventional helicopters (advance ratio μ=0.3) and that is a high advance ratio for future-type helicopters (μ =0.7). The blade tip Mach number for this model is about 0.3 for the main rotor and about 0.48 for the tail propeller.

Table 3 : simulation cases in this study

Inflow speed (Forward flight speed) U_∞	30, 70 m/s 45 m/s (for validation)
Pitch angle of tail propeller θ_{TP}	15~45 deg
Configurations of grid(4types)	TP_iso Fuse_iso TP+MR TP+Fuse (see Figure 1)

2.3. Numerical grid

An overview of the computational grid of CFD is given below. The grid system used in rFlow3D is an overset type. It consists of background grids that resolve the region around the object and a blade/fuselage grid that captures the aerodynamic forces of the rotor blade and the fluctuations generated by the surface of blade and fuselage. The schematic views of grid setting in this study are shown in Figure 2.

The background grid are structural grids. The outer background grid (OBK), which sets the computational domain and boundary conditions for the entire computational space, and the inner background grid (IBK), which captures the area around the rotor blade with high resolution. The grid around the fuselage is modelled as an unstructured grid to deal with complex shapes. Table 3 shows the specifications of the computational grid used in this study, and Table 4 shows the list of the grid used in each case. The spatial resolution of the inner background grid is set based on the main rotor for IBK1 and the tail propeller for IBK2, and is created with a width of 20% of the respective blade chord length(c_{TP} for the tail propeller, c_{MR} for the main rotor), with the outer background grid having about half that resolutions. For the object grid, the wall first layer width is set so that y^+<1.

The total number of grid points is 5.8M for the smallest TP_iso, and 15-16M for TP+MR and TP+Fuse, which are interaction cases.

Table 4 : Specification of computational grids

	domain	# of cells	Min. distance of grids
OBK1	$100\times100\times100$ D_{TP}	101×115×115	$0.4c_{\mathrm{TP}}$
OBK2	$100\times100\times100$ D_{MR}	163×163×129	$0.4c_{\mathrm{MR}}$
IBK1	$2.0\times1.3\times0.75$ D_{MR}	207×163×95	$0.2c_{\mathrm{MR}}$
IBK2	$1.5\times1.5\times1.5$ D_{TP}	117×117×117	$0.2c_{\mathrm{TP}}$
Blade _MR	-	121×121×61	y^+<1
Blade _TP	-	97×149×71	y^+<1
Fuselage	-	5M (unstructured)	y^+<1

Table 5 : computational grids used in each case

	TP_iso	Fuse_iso	TP+MR	TP+Fuse
OBK1	1	-	-	-
OBK2	-	1	1	1
IBK1	-	1	1	1
IBK2	1	-	1	1
Blade_MR	-	-	4	-
Blade_TP	3	-	3	3
Fuselage	-	1	-	1
Total # of cells	5.8M	11M	14.5M	16M

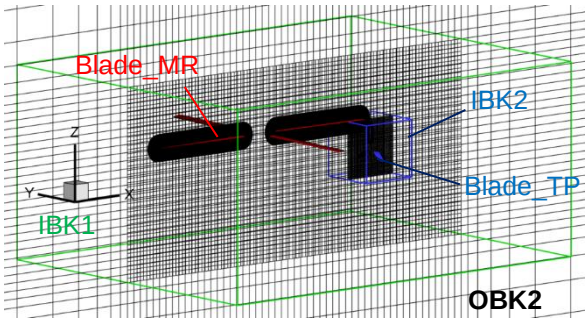

(1) TP/MR

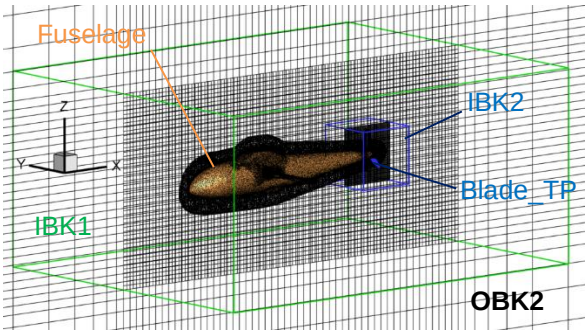

(2) TP/Fuse

Figure 2 : Schematic view of the computational grids

3. RESULTS AND DISCUSSION

3.1. Validation

The performance prediction of the tail propeller is validated by comparing it with the results of the wind tunnel test [14]. The wind tunnel test is shown in Figure 3. The load was measured through the sting attached to the bottom of the fuselage, and the propeller torque was calculated from the current and voltage of the motor used to drive the propeller. Since it was not possible to measure the load of the tail propeller alone, the propeller thrust was derived by subtracting the measured fuselage drag.

Figure 3 : Wind tunnel testing of a compound helicopter model in 2018 [14].

To compare the propeller performance, the thrust coefficients C_T and torque coefficients C_Q are calculated as (1) and (2). where T_{TP} is the propeller thrust, Q_{TP} is the torque, ρ is the density, and n is a rotational speed.

(1) $$C_T = \frac{T_{TP}}{\rho n^2 D_{TP}^4}$$

(2) $$C_Q = \frac{Q_{TP}}{\rho n^2 D_{TP}^5}$$

The thrust and axial torque were obtained by integrating the pressure distribution and frictional stress on the blade in CFD. The obtained results are shown in Figure 4. The thrust was calculated from the balance measurements (with correction for fuselage drag), and the torque is calculated from the motor current-voltage values assuming 100% motor efficiency. When the torques of both are comparable, the torque-thrust curves appear to be approximately the same, although the CFD tends to evaluate thrust more. Since CFD models only the blade portion and does not take into account mechanical losses, it is considered to have a trend to underestimate torque of a propeller. Therefore, the trend of the difference from the experimental values here can be considered reasonable.

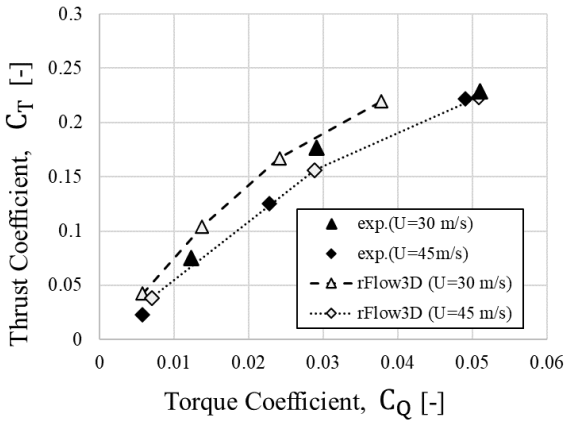

Figure 4 : Torque – Thrust (comparison with wind tunnel test [14])

3.2. Tail propeller - Main rotor Interaction

3.2.1. Propeller performance

From here, the effect of the main rotor on the tail propeller performance is investigated. The aerodynamic performance is evaluated by varying the pitch angle of the tail propeller under two conditions: inflow velocity U_∞= 30 m/s and 70 m/s. The former condition assumes an advance ratio in conventional helicopters, while the latter simulates the high advance ratio in future high-speed helicopters. In a high advance ratio condition, the lift from the fixed wing would have a large proportion of the lift, so the thrust of the main rotor would be reduced. In this study, the main rotor is trimmed to generate 30% of the gross weight.

The thrust generated by the tail propeller concerning the pitch angle is shown in Figure 5. The dashed line shows the conventional advance ratio condition (U_∞= 30 m/s) and the solid line shows the high advance ratio condition (U_∞= 70 m/s).

In comparison with each other, there is a tendency for the thrust to increase due to the influence of the main rotor when the advance ratio is small, while this tendency cannot be confirmed at a high advance ratio.

The propeller efficiency was then calculated according to (3). where $T_{TP}$is propeller thrust, U_∞ is forward speed, Q_{TP} is propeller torque, and Ω is rotational angular velocity.

$$\eta = \frac{T_{TP} U_\infty}{Q_{TP} \Omega} \quad (3)$$

The relationship with the thrust coefficient is displayed in Figure 6. The maximum propeller efficiency is about 70% at U_∞=30 m/s and about 80% at U_∞=70 m/s. The reason for the high propeller efficiency at a high advance ratio is that the propeller is designed to perform well at high-speed flight, where a large amount of thrust is required.

The required thrust for each flight condition can be estimated from the fuselage drag values obtained in previous wind tunnel tests[]: C_T < 0.05 at U_∞= 30 m/s and C_T ~ 0.15 at U_∞ = 70 m/s. Confirming the propeller efficiency in those areas, it can be seen that the propeller performance tends to improve under the conventional advance ratio, however, there is almost no change in the performance under the high advance ratio.

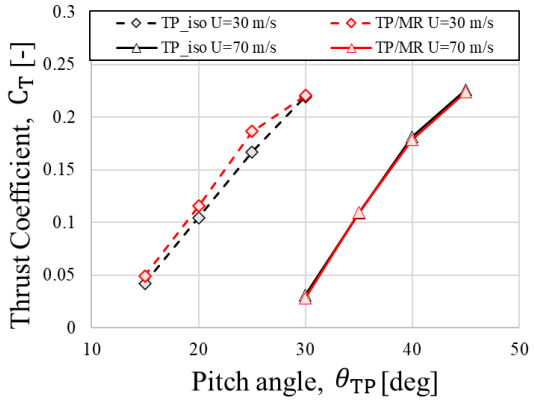

Figure 5 : Pitch angle – Thrust coefficient (with and without main rotor)

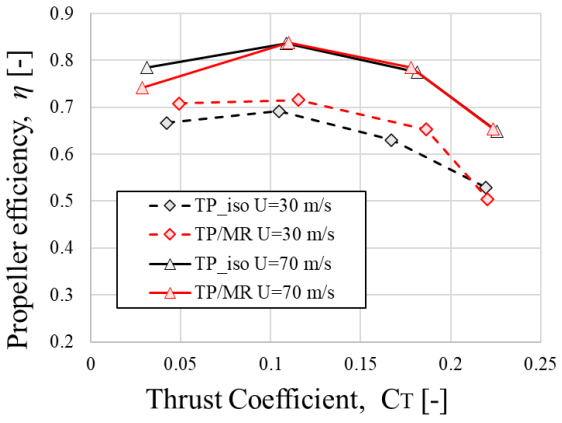

Figure 6 : Thrust coefficient – propeller efficiency(with and without main rotor)

3.2.2. Main rotor wake interaction

Previous studies have shown that a downwash of a main rotor during hovering causes positive effect on propeller performance [15] [16], and it is expected that the performance change observed in this study should be due to the similar effect. U_∞ =30 m/s, θ_{TP}=15deg and U_∞=70 m/s, θ_{TP}=40deg are used as representative cases, vertical velocity distributions around the rotor and propeller are shown in Figure 7. The vertical velocity w is normalized by the speed of sound. As the advance ratio increases, a main rotor wake, including the blade tip vortex, move almost directly behind the rotor, and would flow away without any significant external influence on the tail propeller inflow. Focusing on the velocity distribution around the tail propeller, it seems that the effect of the downwash of the main rotor is weakened by the increase in the advance ratio. In addition, as the forward flight speed increases, the magnitude of the wind fluctuation generated by the main rotor wake becomes relatively small, and it can be inferred that it does not cause significant changes in a propeller performance.

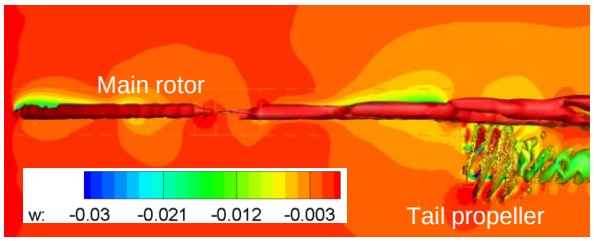

TP/MR, U_∞ = 30 m/s, θ_{TP} = 15 deg

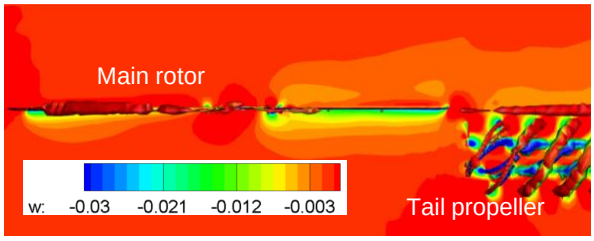

TP/MR, U_∞ = 70 m/s, θ_{TP} = 40 deg

Figure 7 : Vertical velocity distribution (vorticity iso-surfaces are shown together)

3.3. Tail propeller - Fuselage interaction

3.3.1. Propeller performance

Next, the aerodynamic interactions between the tail propeller and the fuselage are investigated. First, the thrust for each pitch angle condition is checked in Figure 8. It can be seen that the thrust at the same pitch angle is increased compared to the isolated condition. The increment is larger at U_∞= 30 m/s (indicated by the dashed line in the graph).

Presented at 47th European Rotorcraft Forum, United Kingdom, 7-9th September, 2021

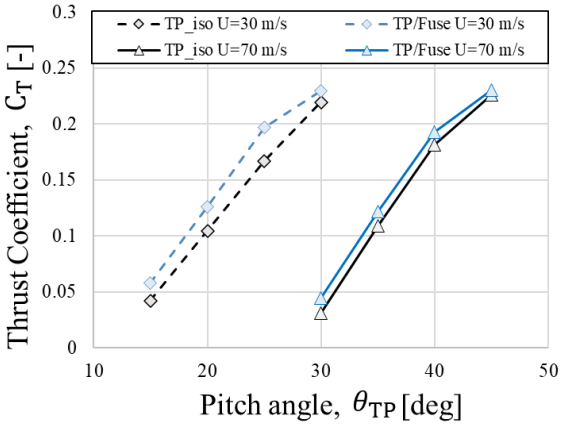

Figure 8 : Pitch angle – Thrust coefficient (with and without Fuselage)

The propeller efficiency is then shown in Figure 9. The efficiency improved with the increase in thrust. When the propeller interfered with the main rotor, the change in performance became smaller under the high advance ratio condition (U_∞= 70 m/s), but when it interfered with the fuselage, the propeller performance changed regardless of the advance ratio. This difference is due to the different mechanisms of aerodynamic interactions. Since the main rotor induces flow in the vertical direction, the advection direction of the wake changes depending on the advance ratio, and the degree of influence on the propeller changes, however in the case of interaction with the fuselage, the fuselage shadow is the main factor for interactions. It affects the entire rotating surface regardless of the advance ratio, and the dependence on the advance ratio is considered to be small.

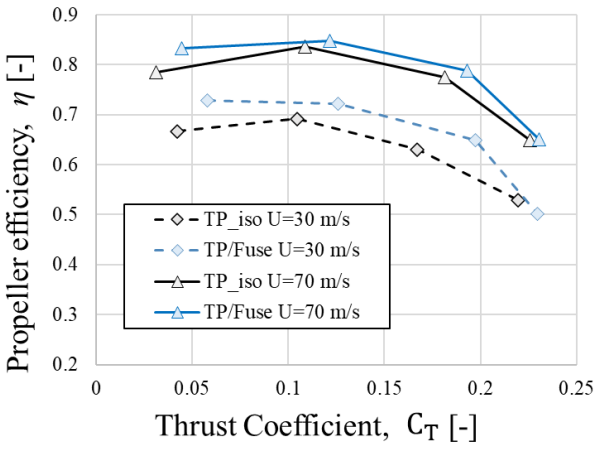

Figure 9 : Thrust coefficient – propeller efficiency(with and without Fuselage)

To confirm this, the main direction velocity distribution around the fuselage in the Fuse_iso case is shown in Figure 10. Compared to the forward flight speed, there is a large decrease around the tail propeller in both flight conditions. It infers a large change in the inflow wind speed to the tail propeller surface from the isolated propeller analysis.

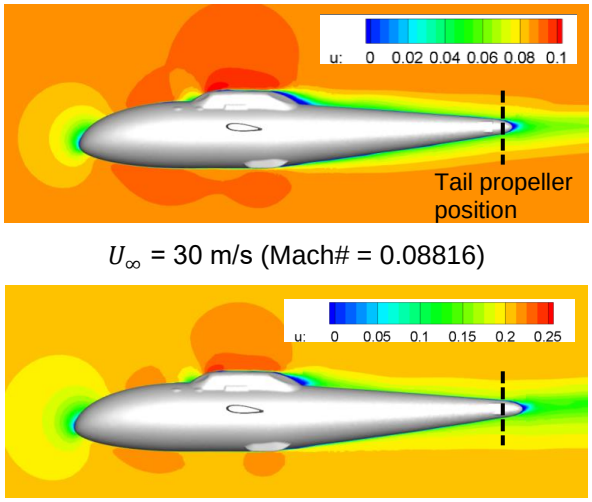

Figure 10 : Velocity of mainstream direction in isolated Fuselage cases

3.3.2. Effect on fuselage drag

Since the propeller gives momentum to the air flowing into the rotating surface and increases its speed, it should affect the flow field around the fuselage and change the fuselage drag. To confirm this, section A is set at a position upstream from the tail propeller position by the propeller radius R_{TP}, and the mainstream directional distribution at this position is obtained (Figure 11). The comparison of wind speed between the isolated fuselage (Fuse_iso) and with a propeller (TP+Fuse) is depicted in Figure 12.

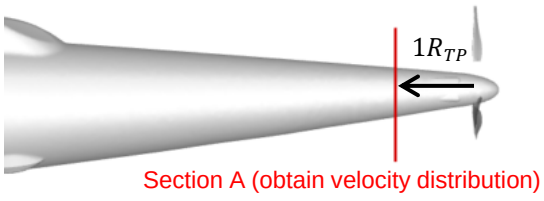

Figure 11 : Cross-sectional position for obtaining wind speed

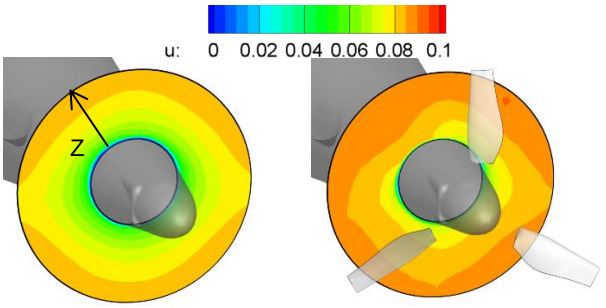

Fuse_iso TP/Fuse (θ_{TP}=15deg)

(1) U_∞ = 30 m/s

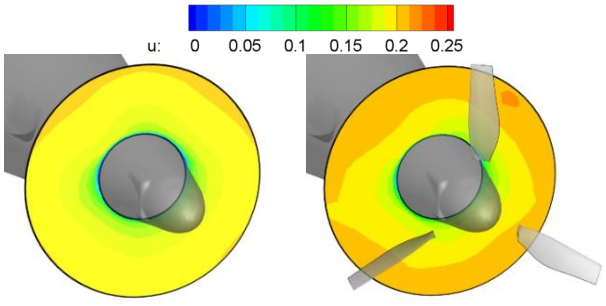

Fuse_iso TP/Fuse (θ_{TP}=40deg)

(2) U_∞ = 70 m/s

Figure 12 : Change in velocity in the mainstream direction around the fuselage due to the tail propeller (contours at section A in Figure 11)

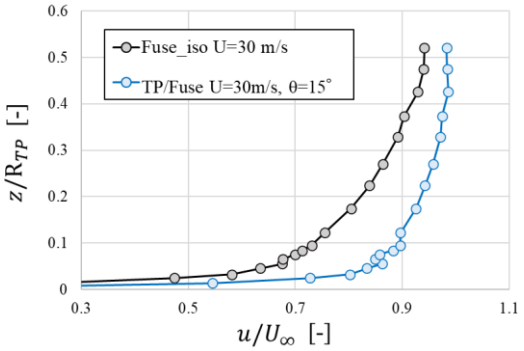

(1) U_∞ = 30 m/s

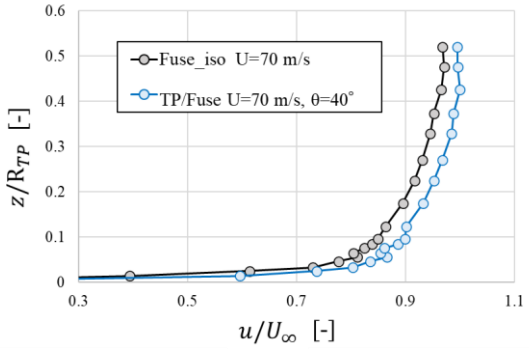

(2) U_∞ = 70 m/s

Figure 13 : Mainstream velocity profiles in the wall wise direction (at Section A in Figure 11, calculated by circumferentially averaging distributions in Figure 12)

To confirm the wind speed distribution shown in Figure 12 more quantitatively, the wind speed in wall-wise direction U is calculated by taking the wall distance z from the wall to the far region and averaging them in the circumferential direction. Figure 13 shows the results. The horizontal axis is the wind speed, which is normalized by the forward flight speed, and the vertical axis shows the wall distance, which is non-dimensionalized by the propeller radius.

When the increment from Fuse_iso to TP+Fuse is focused on, it can be confirmed that the increment is about 15% of the forward flight speed at z/R < 0.2 in the moderate advance radio. In the high advance ratio condition (U_∞ = 70 m/s), the increment is about 5% of the forward flight speed. It is thought that the pressure and frictional stress distributions on the fuselage surface change due to the thinning of the boundary layer around the wall.

An example of the change in surface pressure and frictional stress distributions due to the propeller-induced speed increase is displayed in Figure 14 and Figure 15 for U_∞=30 m/s. Note that each value is normalized using the speed of sound. They show that the pressure tends to become smaller and the friction stress tends to increase due to the propeller. Since the pressure difference between the head and tail of the fuselage leads to the fuselage drag, it is obvious that these changes are all contributing to the increase of the fuselage drag.

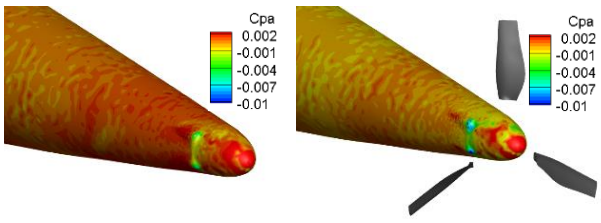

Fuse_iso TP/Fuse

Figure 14 : Pressure contours on the fuselage wall around the tail propeller (U_∞ = 30 m/s)

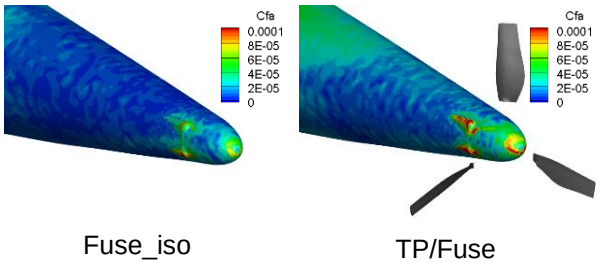

Figure 15 : Frictional stress contour on the fuselage wall around the tail propeller ($U\infty$ = 30 m/s)

The incremental fuselage drag due to these changes in surface distributions is summarized in Figure 16. In all cases, the increment is about 80 counts, which is less than 10% compared to the overall fuselage drag. The relatively small increment in frictional drag under the condition of U=70m/s is due to the small difference in velocity change as seen in the velocity distribution earlier(Figure 13), and is thought to be due to the prevailing effect of negative pressure caused by the increased propeller thrust.

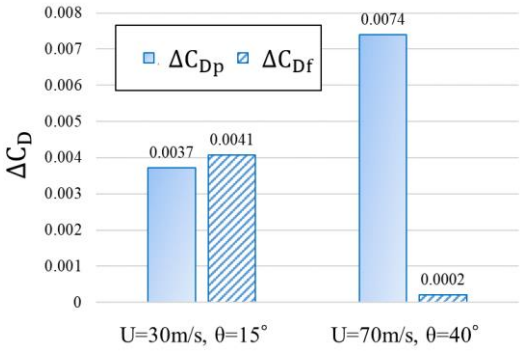

Figure 16 : Change in the fuselage drag due to the tail propeller interaction

3.3.3. Impact on aircraft system

For the tail propeller-to-fuselage interactions, the qualitative results for each component are as follows

1 : Propeller thrust and efficiency are improved.

2 : Fuselage drag is increased.

These are conflicting effects. Therefore, it is necessary to subtract the effects of each of these two factors to confirm the effect on the overall airframe system. By subtracting the increase in fuselage drag from the increase in propeller thrust, as shown in (4) and Figure 17, the effective thrust of the tail propeller can be introduced.

$$T_{\text{eff}} = T_{\text{TP\_iso}} + \Delta T_{TP} - \Delta D_{Fuse} \quad (4)$$

where ΔD_{Fuse} is the incremental drag of fuselage obtained by subtracting the drag in the interaction case from the drag in the isolated fuselage case.

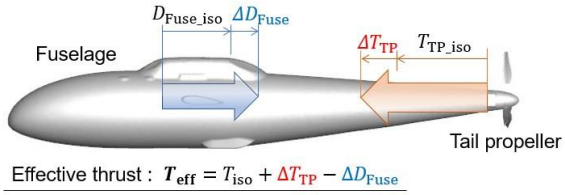

Figure 17 : the concept of an effective thrust considering interactions

The propeller thrust and efficiency are again evaluated using this effective thrust and are shown in Figure 18 and Figure 19. In the case where only the thrust is focused on, it seems that the thrust at the same pitch angle is the same or tends to increase even when the increment in fuselage drag is taken into account. However, under the high advance ratio conditions, the thrust is almost the same as that of the isolated propeller, indicating that the increase in fuselage drag and the increase in propeller thrust cancel each other out. This is because the increase in fuselage drag is proportional to the square of the forward flight speed, and the contribution of fuselage drag becomes relatively larger.

In terms of propeller efficiency, it tends to decrease under the high advance ratio condition. Even if the increase in propeller thrust can cancel out the increase in fuselage drag, the increase in the propeller torque at the same time results in a decrease in the propeller efficiency. In other words, it can be understood that in a design that aims for high-speed forward flight using a tail propeller, it is necessary to pay attention to the increase in propeller power, especially at the maximum forward speed.

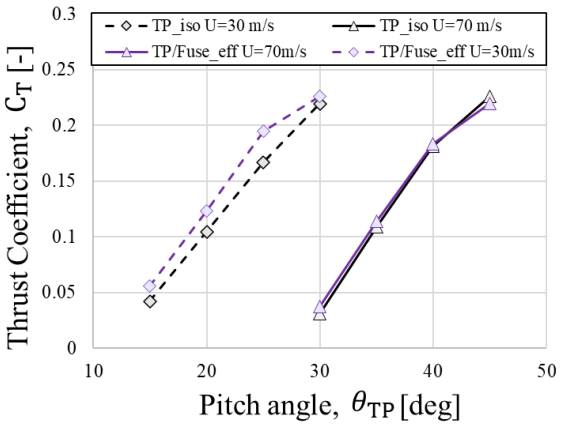

Figure 18 : Pitch angle – Thrust coefficient (isolated vs effective value taking into account increased fuselage drag)

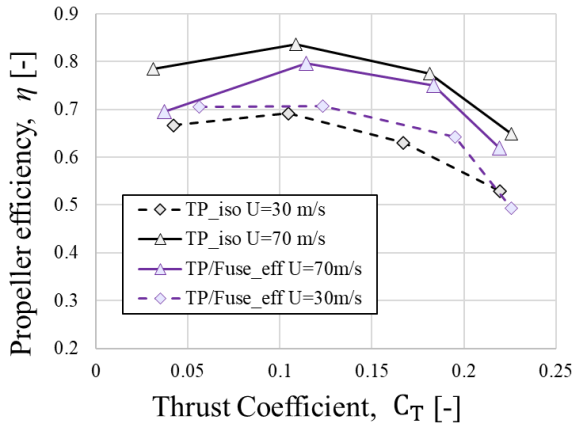

Figure 19 : Thrust coefficient – propeller efficiency (isolated vs effective value taking into account increased fuselage drag)

4. CONCLUSIONS

The aerodynamic interactions between the tail propeller and the main rotor & fuselage are investigated using CFD for a high-speed compound helicopter model being considered by JAXA. The conclusions are summarized below.

・The advection direction of the main rotor wake during forward flight becomes directly behind the main rotor as the advance ratio increases. Therefore, interactions with the tail propeller is weakened at high advance ratios (when a propeller is located below the tip pass plane of the main rotor).

・The performance of the tail propeller increases as it enters the shadow of the fuselage. This is due to the fact that the propeller is placed in an area of low wind speed, which allows it to more easily increase the speed of the surrounding area and generate the same amount of thrust with less power.

・The thrust generated by a tail propeller increases the velocity of the flow field around the aft of a fuselage and increases the flow velocity near the wall. As a result, the fuselage drag increases due to the increase in frictional stress and decreases of the pressure around the wall.

・ The aerodynamic interactions between the fuselage and the tail propeller produces the conflicting effects of increased fuselage drag and increased propeller thrust, and when considering the overall effect of these factors on the entire aircraft, there is a great possibility that the propeller efficiency will decrease as the advance ratio becomes high.

Based on these results, we will study the case where the main rotor and the fuselage interfere with the tail propeller at the same time, simulate the interaction case with the tail horizontal/vertical wings that are omitted this time, and search for more optimal conditions for the propeller placement to maximize the effects of interactions in a positive direction.

REFERENCES

[1] "LOCKHEED MARTIN HP," [Online]. Available: https://www.lockheedmartin.com/en-us/products/s-97-raider.html. [Accessed 12 7 2021].

[2] "LOCKHEED MARTIN HP," [Online]. Available: https://www.lockheedmartin.com/en-us/products/sb1-defiant-technology-demonstrator.html. [Accessed 12 7 2021].

[3] D. Walsh, S. Weiner, A. Bagai, T. Lawerence , R. Blackwell, “Development Testing of the Sikorsky X2 Technology Demonstrator, ” American Helicopter Society 65th Annual Forum, 2009.

[4] Airbus, "Airbus Helicopters reveals Racer high-speed demonstrator," 20 6 2017. [Online]. Available: https://www.airbus.com/newsroom/press-releases/en/2017/06/Airbus-Helicopters-reveals-Racer-high-speed-demonstrator-configuration.html. [Accessed 11 7 2021].

[5] Y. Tanabe, T. Aoyama, N. Kobiki, M. Sugiura, R. Miyashita, S. Sunada, K. Kawachi , M. Nagao, “A Conceptual Study of High Speed Rotorcraft,” 40th European Rotorcraft Forum, Southampton, UK, September, 2014.

[6] T. Stokkermans, L. Veldhuis, B. Soemarwoto, R. Fukari , P. Eglin, “ Breakdown of aerodynamic interactions for the lateral rotors on a compound helicopter, ” Aerospace Science and Technology, 101, 105845., 2020.

[7] G. J. Leishman, “ Principles of helicopter aerodynamics,” Cambridge university press, 2006.

[8] H. Sugawara, Y. Tanabe , M. Kameda, “Influence on Aerodynamic Performance of a Compound Helicopter by Wing Incidence Angle,” Transactions of JSASS, Vol.67, No.3, pp.93-101, 2019.

[9] S. Yamamoto , H. Daiguji, “Higher-Order-Accurate Up-wind Schemes for Solving the Compressible Euler and Navier-Stokes

Equations," Computers & Fluids 22.2-3, 259-270, 1993.

[10] E. Shima , K. Kitamura, "On New Simple Low-Dissipation Scheme of AUSM-Family for All Speeds," 47th AIAA Aerospace Sciences Meeting Including the New Horizons Forum and Aerospace Exposition , 2009.

[11] Y. Tanabe , S. Saito, "Significance of All-Speed Scheme in Application to Rotorcraft CFD Simulations," 3rd International Basic Research Conference on Rotorcraft Technology, Nanjing, China, October 14-16, 2009.

[12] A. Hashimoto, K. Murakami, T. Aoyama, K. Ishiko , M. Hishida, "Toward the fastest unstructured CFD code 'FaSTAR'," Proc. of 50th AIAA Aerospace Sciences Meeting Including the New Horizons Forum and Aerospace Exposition,Nashville, Tennessee, AIAA-2012-1075, 2012.

[13] Y. Tanabe, S. Saito , H. Sugawara, "Evaluation of Rotor Noise Reduction by Active Devices Using a CFD/CSD Coupling Analysis Tool Chain," Proceedings of 1st Asian/Australian Rotorcraft Forum, ARF 2012 Executive Committee Paper A-IV-1_P107_F, Busan, K,, 2012.

[14] N. Kobiki, Y. Tanabe, M. Sugiura, H. Sugawara , K. Kimura, "An Aerodynamic Study for the 3rd Configuration of JAXA High Speed Compound Helicopter," 58th aircraft symposium, 3B07, 2020.

[15] K. Kimura, H. Sugawara , Y. Tanabe, "Aerodynamic interaction between main rotor and Side Propellers of a compound helicopter," 58th aircraft symposium, 3B08, 2020.

[16] F. Frey, C. Öhrle, J. Thiemeier, M. Keßler , E. Krämer, "Aerodynamic Interactions on Airbus Helicopters' Compound Helicopter RACER in Hover," In VFS International 76th Annual Forum & Technology Display, AHS International 74th Annual Forum & Technology Display, Vertical Flight Soc. Paper (pp. 76-2020)., 2020.

Presented at 47th European Rotorcraft Forum, United Kingdom, 7-9th September, 2021